RELIEF MAPPING ON CUBIC CELL COMPLEXES

Karl Apaza, Carlos Andujar
MOVING Group, Universitat Politecnica de Catalunya, Barcelona, Spain
kapazag@gmail.com, andujar@lsi.upc.edu

Keywords: Displacement mapping, Relief mapping, GPU Raycasting, Quadrilateral parameterization

Abstract: In this paper we present an algorithm for parameterizing arbitrary surfaces onto a quadrilateral domain defined by a collection of cubic cells. The parameterization inside each cell is implicit and thus requires storing no texture coordinates. Based upon this parameterization, we propose a unified representation of geometric and appearance information of complex models. The representation consists of a set of cubic cells (providing a coarse representation of the object) together with a collection of distance maps (encoding fine geometric detail inside each cell). Our new representation has similar uses than geometry images, but it requires storing a single distance value per texel instead of full vertex coordinates. When combined with color and normal maps, our representation can be used to render an approximation of the model through an output-sensitive relief mapping algorithm, thus being specially amenable for GPU raytracing.

1 INTRODUCTION

During the last few decades much research effort has been devoted to build parameterizations between polygonal meshes and a variety of domains, including planar regions, triangular or quadrilateral meshes, polycubes and spheres. The parameterization literature has focused mainly on minimizing distortion, guaranteeing global bijectivity, and producing seamless parameterizations for complex surfaces. With very few exceptions, parameterization methods for computer graphics compute piecewise linear mappings that must be encoded explicitly, typically by associating a pair of texture coordinates (u,v) to each vertex. The explicit nature of these parameterizations makes them non-reversible, i.e. computing the point in the mesh represented by a point (u,v) in parameter space is a costly operation, unless additional data structures are used (García and Patow, 2008). One notable exception are Geometry Images (Gu et al., 2002; Losasso et al., 2003), which allow representing geometric and appearance details such as color/normal data as separate 2D arrays, all of them sharing the same implicit surface parametrization and thus requiring no texture coordinates.

In this paper we present a method to define projection-based parameterizations of arbitrary surface meshes onto a quadrilateral domain formed by a subset of the faces of the cubic cells intersected by the mesh (Figure 1). The resulting parameterizations are implicit and allow representing geometric and appearance details using a collection of 2D arrays. Unlike geometry images though, points (u,v) on our quadrilateral domain have associated a point $P' = (x',y',z')$ in 3D space (on the face of a cubic cell). This fact, along with a projection-based parameterization, allows (a) encoding the coordinates of surface points $P = (x,y,z)$ with a single distance value $||P-P'||$ instead of storing global (x,y,z) coordinates in the 2D array, and (b) computing quickly the intersection of arbitrary rays with the mesh implicitly encoded by the above distance maps.

Since we target GPU-based construction and rendering algorithms, we restrict ourselves to easily invertible, implicit projections. Given a point (u,v) on the domain, we can easily compute the direction towards the mesh point mapped to (u,v). We use four different projection types (parallel, perspective, axial and planar) which are chosen on a cell-basis, according to the local neighborhood of the cell. These pro-

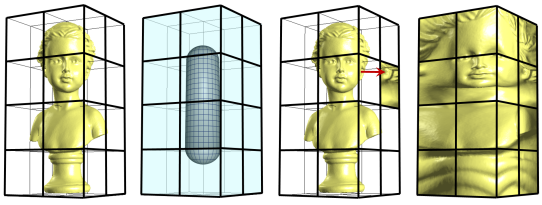

(a) (b) (c) (d)

Figure 1: Overview of our approach: (a) set of cells intersected by the surface mesh; (b) the direction of projection is defined by the normals of the shown surface; (c) each point inside the cells is mapped onto a point on the external faces; (d) mesh projected onto the external faces.

jections map any point (x,y,z) inside the cubic cell onto a point (x',y',z') on one of its faces, which in turn can be expressed in local coordinates (u,v) inside the face, see Figure 1(c).

Given an arbitrary surface mesh, we compute a set of cubic cells and, using the implicit parameterization, we sample the input mesh to fill in the 2D arrays with attributes such as distance, normal and color data. Each attribute is stored as an array texture. This provides a unified representation of the surface mesh which allows extracting a level-of-detail approximation of the original surface. Like geometry images, our representation can be rendered using a geometry-based approach suitable for rasterization-based visualization, which involves unprojecting each texel using the implicit projection and the stored distance value. Moreover, a unique feature of our representation is that it is amenable for raycasting rendering, using a GPU-based algorithm with a pattern similar to that of relief mapping algorithms. This last rendering approach makes our representation specially suitable for raytracing in the GPU.

The rest of the paper is organized as follows. Section 2 reviews previous work on implicit parameterizations and relief mapping techniques. Our projection-based parameterization and the way we use it to construct and render detailed meshes are discussed in Section 3. Section 4 discusses our results on several test models. Finally, Section 5 provides concluding remarks and future work.

2 PREVIOUS WORK

In recent years a number of methods for parameterizing meshes have been proposed, targeting multiple parameter domains and focusing on different parameterization properties such as minimizing distortion and guaranteeing global bijectivity. Most methods developed so far target a planar domain and thus require cutting the mesh into disk-like charts to avoid excessive distortions and to make the topology of the mesh compatible to that of the domain (see (Floater and Hormann, 2005; Sheffer et al., 2006) for a recent survey). Parameterizations onto more complex domains such as triangle or quadrilateral meshes avoid cutting the mesh and thus provide seamless parameterizations. A popular base domain are simplicial complexes obtained e.g. by just simplifying the original triangle mesh (see e.g. (Lee et al., 1998; Guskov et al., 2000; Praun et al., 2001; Purnomo et al., 2004)), allowing each vertex of the original mesh to be represented with barycentric coordinates inside a vertex, edge, or face of the base domain. Some recent approaches target quadrilateral instead of triangle meshes (Tarini et al., 2004; Dong et al., 2006). Polycube maps (Tarini et al., 2004) use a polycube (set of axis-aligned unit cubes attached face to face) as parameter domain. Each vertex of the mesh is assigned a 3D texture position (a point on the surface of the polycube) from which a simple mapping is used to look up the texture information from the 2D texture domain. Construction of the parameterization involves (a) finding a proper polycube roughly resembling the shape of the given mesh, (b) warping the surface of the polycube so as to roughly align it with the surface mesh, (c) projecting each mesh vertex onto the warped polycube along its normal direction, (d) applying the inverse warp function to the projected vertices, and (e) optimizing the texture positions by an iterative process. Unfortunately, no automatic procedure is given for steps (a) and (b), which are done manually. Our approach also targets a domain formed by axis-aligned quadrilateral faces, but differs from polycube maps in two key points: our parameterization is implicit and thus does not require storing texture coordinates, and it is easily invertible and thus it is amenable to raycasting rendering.

Gu et al. (2002) propose to remesh an arbitrary surface onto a completely regular structure called Geometry Image which captures geometry as a simple 2D array of quantized point coordinates. Other surface attributes like normals and colors can be stored in similar 2D arrays using the same implicit surface parametrization. Geometry images are built cutting the mesh and parameterizing the resulting single chart onto a square. Geometry images have been shown to have numerous applications including remeshing, level-of-detail rendering and compression. Our representation has similar uses than geometry images, although construction is much simpler and requires encoding only distance values instead of full vertex coordinates.

Solid textures (Perlin, 1985; Peachey, 1985) avoid the parameterization problem by defining the texture inside a volume enclosing the object and using directly the 3D position of surface points as texture coordinates. Octree textures (Benson and Davis, 2002) strive to reduce space overhead through an adaptive subdivision of the volume enclosing the object. Although octree textures are amenable for GPU decoding (Lefebvre et al., 2005), a subdivision up to texel level (each octree leaf representing a single RGB value) causes many unused entries in its nodes, thus limiting the maximum achievable resolution. Space overhead grows even further when using N^3-trees or page tables to reduce the number of texture indirections (Lefebvre et al., 2005; Lefohn et al., 2006). TileTrees (Lefebvre and Dachsbacher, 2007) also rely on an octree enclosing the surface to be textured, but instead of storing a single color value at the leaves, square texture tiles are mapped onto leaf faces. Resulting tiles are compactly stored into a regular 2D texture. During rendering, each surface point is projected onto one of the six leaf faces, depending on surface orientation. The resulting texture has little distortion and is seamlessly interpolated over smooth surfaces. We also use projection onto cell faces, but our work differs from TileTrees in two key aspects. On the one hand, we do not restrict ourselves to parallel projection; we also use perspective and axial projections whenever appropriate. On the other hand, our approach is suitable for encoding geometry as displacement maps. Note that this does not apply to TileTrees because determining the face a surface point P inside a cell must be projected onto requires knowledge about both the P coordinates and its normal vector.

Relief mapping (Policarpo et al., 2005) has been shown to be extremely useful as a compact representation of highly detailed 3D models. All the necessary information for adding surface details to polygonal surfaces is stored in RGBA textures, with the alpha channel storing quantized depth values. The technique uses an inverse formulation based on a ray-heightfield intersection algorithm implemented on the GPU. For each ray, the intersection is found by a linear search followed by a binary search along the ray. This algorithm has been extended in (Policarpo and Oliveira, 2006) to render non-height-field surface details in real time. This new technique stores multiple depth and normal values per texel and generalizes their previous proposal for rendering height-field surfaces. Baboud and Décoret (Baboud and Décoret, 2006) obtain more accurate intersections than the linear search of (Policarpo et al., 2005) by precomputing a safety radius per-texel, this way larger steps can be made. Moreover, the height fields are built using inverse perspective frusta, which help improve the sampling on certain regions. Omni-directional relief impostors (Andujar et al., 2007) represent surface meshes by pre-computing a number of relief mapped polygons distributed around the object. In runtime, the current view direction is used to select a small subset of the pre-computed maps which are then rendered using relief mapping techniques.

The relationship of our approach with displacement and relief maps is twofold. On the one hand, displacement mapping also relies on a simple projection (parallel projection) plus depth values to encode fine geometric details. On the other hand, all acceleration techniques for computing the intersection of a ray with the surface implicitly encoded by the distance map can be adopted to render our representation, by just projecting each sample along the ray onto the texture domain. These acceleration methods include, among others, linear search plus binary search refinement (Policarpo et al., 2005), varying sampling rates (Tatarchuk, 2006), and precomputed distance maps (Baboud and Décoret, 2006; Donnelly, 2005).

3 OUR APPROACH

3.1 Notation

Let M be the input mesh, and let $\mathcal{V}$ be the set of cubic cells in an $N \times N \times N$ grid subdivision of the axis-aligned bounding cube of M. Cells in $\mathcal{V}$ can be classified as white (W) cells (those outside M), black (B) cells (those inside M), and grey (G) cells (those with non-empty intersection with the boundary of M). A face of a G cell shared with a W cell will be referred to as *external face*. Otherwise it will be called *internal face*. A G cell has between zero and six external faces. G cells with at least one external face will be referred to as *border G cells* (BG cells for short). Likewise, G cells with no external faces will be referred to as *interior G cells* (IG cells).

3.2 Parameterization

Our mapping is based on projecting the boundary of M onto the external faces of BG cells and the internal faces of IG cells. We will collectively refer to these faces as *domain faces*. Each G cell is assigned a projection type which projects points inside the cell onto the subset of domain faces of the cell. According to the internal/external status of its six faces, a G cell can have one out of 2^6 configurations, which can be grouped under rotations into ten base cases (Figure 4).

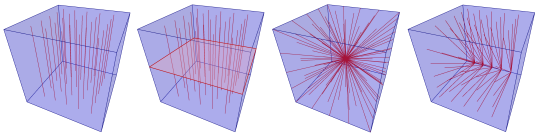

Figure 2: The four types of projections we consider inside each cell: (a) parallel, (b) planar, (c) perspective, (d) axial.

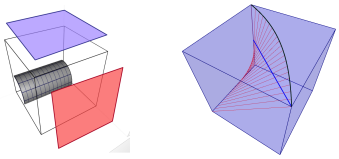

Figure 3: The axial parameterization maps straight line segments onto planar curves. A sample case using axial projection from the bottom back edge onto two external faces (*left*); this projection maps the blue segment onto a planar curve on the top face of the cubic cell (*right*).

We use four different projection types (Figure 2):

- Parallel projection: defined by a vector $\vec{v}$ establishing the direction of projection (DoP).
- Planar projection: defined by a plane Π with equation $ax+by+cz+d=0$. A point P inside the cell will be projected along the normal $\vec{n}=(a,b,c)$ or the opposite normal $-\vec{n}$ depending on the halfspace where P is located, i.e. depending on the sign of $\vec{n}P+d$.
- Perspective projection: defined by a point C establishing the center of projection (CoP). A point P inside the cell will be projected along the direction $\overline{CP}$.
- Axial projection: defined by an axis a parallel to one of the coordinate axes. For example, points on an axis parallel to the X axis has points with the form (λ,a_y,a_z) for some $\lambda\in\mathbb{R}$. A point P inside the cell will be projected along the direction $(\lambda,P_y-a_y,P_z-a_z)$.

In all cases points inside the cell are projected onto the cell's faces. The first three types of projections define linear mappings, projecting mesh triangles inside the cell onto triangles on the support plane of each domain face, whereas the last projection type leads to a non-linear mapping, projecting mesh triangles onto triangular patches with curved edges (Figure 3). This non-linearity property poses no problem to the rendering algorithm, as discussed below.

Each parameterization is local to a cell c in the sense that each G cell has a single projection type, and only the geometry inside a G cell is projected onto its domain faces. We now discuss, for each base case, the type of projection we use, which constraints affect the parameter $(\vec{v},C,\Pi,a)$ controlling the projection (so as to guarantee that points inside the cell are projected only onto its domain faces), and how to compute a suitable value for that parameter (Figure 5).

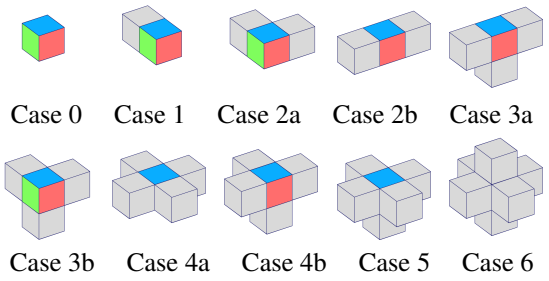

Figure 4: Configurations of a G cells can be grouped into the ten base cases shown. For each case we show a G cell (with colored faces) and its non-empty 6-connected cells.

Case 0. All six faces are external. We use a perspective projection with the CoP C being any point inside the cell. This point can be computed simply as the cell's center.

Case 1. All faces are external except for one internal face F. We also use a perspective projection, this time C being any point on F. Our current implementation computes C as the middle point of F.

Case 2a. All edges are shared by external faces, except for one internal edge e. Again, we use perspective projection with C being any point on e. Our implementation uses the middle point of e.

Case 2b. Only two internal faces F_1,F_2 in opposite directions. We use an axial projection, taking any axis defined joining a point on F_1 with a point on F_2. Our current implementation uses the axis defined by joining the middle points of F_1 and F_2 .

Case 3a. Three external faces and only two internal edges e_1,e_2. We also use an axial projection, with the axis defined by joining a point on e_1 and a point on e_2. Our current implementation simply uses the midpoints of e_1 and e_2.

Case 3b. Three internal faces meeting at a vertex v. We use perspective projection from v.

Case 4a. This case is the complementary of case 2b, with two parallel external faces F_1,F_2. We use a planar projection with Π being a plane parallel to $F_1$and F_2. Our current implementation uses the plane going through the cell's center.

Case 4b. This case is the complementary of case 2a, with a single external edge e_1. For this case we use the axial projection provided by the opposite edge in the cell.

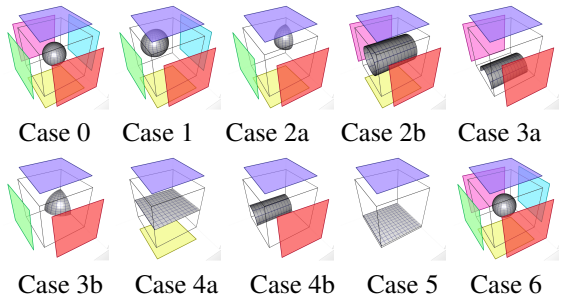

Figure 5: Projection type for each basic G cell configuration. Points inside each G cell are projected onto the colored faces using projection lines perpendicular to the shown spherical/cylindrical/planar surface.

Case 5. This case is the complementary of case 1, with a single external face F. We use a parallel projection with $\vec{v}$ being the normal of F.

Case 6. This case, which is the complementary of case 0, is handled using the same perspective projection.

3.3 Construction

We first assume that a given grid resolution N has been fixed and discuss how to compute the G cells of the resulting $N \times N \times N$ grid (Section 3.3.1), and how to sample properties to build the texture using the projections described above (Section 3.3.2). Then, a simple algorithm for choosing a proper value for N is presented in Section 3.3.3.

3.3.1 Computing the G cells

This step simply accounts for dividing the bounding cube of the input mesh M into an $N \times N \times N$ grid, and classifying the resulting cubic cells as W, G or B. This can be done either in the CPU, following the discretization algorithm described in (Andujar et al., 2002), or in the GPU, using a voxelization algorithm (Eisemann and Décoret, 2008). Our current implementation uses the CPU-based approach because it also provides, for each G cell, the list of faces intersecting it, which greatly accelerates the sampling of surface attributes discussed below.

3.3.2 Sampling surface properties

We now describe a GPU-based algorithm for sampling surface properties to fill the 2D texture associated with each domain face. The algorithm traverses all G cells $\{c_i\}$ and all the domain faces of each c_i. The basic idea is to render the geometry inside the cell onto a texture, using a shader for computing the projection.

The CPU-based part of the rendering algorithm proceeds through the following steps:

1. Setup a frame buffer object (FBO) and a viewport transformation matching the desired texture size.
2. Setup an orthographic camera facing the domain face c_i to be sampled.
3. Set the uniform variables encoding the cubic cell and its projection type, to make this information available to the geometry and fragment shaders.
4. Draw the mesh triangles intersecting the cell.

The vertex shader leaves the input vertices untransformed, the projection being performed in a geometry shader. We have adopted this solution because, due to the non-linearity of the mapping used for cases 2b, 3a and 4b, mesh triangles must be tessellated by subdividing large mesh edges prior to projecting its vertices. The geometry shader thus performs these steps:

1. If the current cell uses axial projection (cases 2b, 3a, 4b), tessellate the triangle by uniformly subdividing the edges longer than a user-defined threshold.
2. Use the projection type to project the vertices into the *support plane* of the domain face c_i to be filled. For mesh triangles whose projection spans multiple domain faces, some projected vertices might lie outside the domain face, but OpenGL's clipping will take care of these cases.
3. For each primitive, emit the projected vertices, encoding its original position as texture coordinates.

Finally, the fragment shader simply encodes in the output color the attribute to be sampled. Distance maps simply encode the distance between mesh points $P = (x, y, z)$ and their projection $P' = (x', y', z')$. Note that these distances must be computed on a per-fragment basis, as they do not interpolate linearly when using e.g. perspective projection (cases 0, 1, 2a, 3b, Figure 5). Since the mapping is non-bijective, multiple surface points might project onto the same texel. In these cases the texel must encode the distance to the closest surface point. This is accomplished by simply setting the fragment depth to the computed distance, so that OpenGL's depth test will discard occluded samples. Other surface signals such as color and normal data are sampled in a similar way (Figure 6).

3.3.3 Choosing a proper grid size

A fine grid provides a better approximation of the surface mesh, each G cell having a simpler region inside

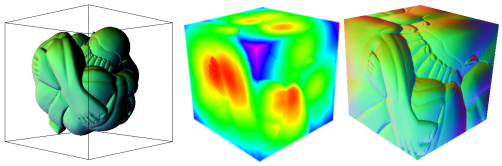

(a) (b) (c)

Figure 6: Sampling attribute values: (a) model inside a single cubic cell; (b) sampled distance $||P-P'||$ represented as color temperature; (c) sampled normals.

and thus more likely to be represented faithfully by the distance maps. However, increasing the number of cells also increases storage space and adds some overhead to the rendering algorithm. Our algorithm for choosing a proper grid resolution N strives to minimize the number of surface elements that map onto the same texel. A simple estimation for this number can be computed by running the sampling algorithm above but using the stencil buffer to count the number of fragments projecting onto the same texel. So we start with an $1 \times 1 \times 1$ grid and compute the ratio of occluded fragments. If the ratio is above a user-defined threshold, we increase (e.g. doubling) the resolution in each direction and repeat the above steps until the ratio is below the threshold, or a maximum N_{max} is reached.

3.4 Representation

Our representation consists of:

- A lookup table encoding the G cells, and the projection type for each G cell.
- A collection of 2D textures (one for each domain face) encoding the distance maps. Since all these textures have the same size, they can be packaged as an array texture (GL_EXT_texture_array extension). An array texture is accessed by shaders as a single texture unit. A single layer is selected using the r texture coordinate, and that layer is then accessed as though it were a 2D texture using (s,t) coordinates.
- An array texture for each additional surface signal (color, normal).

3.5 Rendering

Our representation can be rendered using both a direct approach which reconstructs a triangle mesh approximating the object on-the-fly, or a raycasting approach which relies on intersecting viewing rays with the distance maps.

3.5.1 Geometry-based rendering

Our representation can be rendered by reconstructing a triangle mesh on the fly using an algorithm similar to that of Geometry Images (Gu et al., 2002). The idea is to visit all texels of the distance maps and create a pair of triangles for each 2x2 group of texels. Each texel (u,v) of a domain face is associated with a point $P' = (x',y',z')$ on the surface of a G cell, which can be computed by a simple transformation from local to global coordinates. Using the distance d stored at texel (u,v) and the projection type of the G cell, we can unproject point P' to get a point of the surface mesh. Level-of-detail rendering is implemented by mip-mapping the distance maps. During rendering, the normal-map signal is rasterized over the triangles by hardware, using bilinear filtering of each quad in the normal map. This reconstruction type allows our representation to have similar uses than geometry images.

3.5.2 Raycasting rendering

A more interesting feature of our representation is the output-sensitive rendering through raycasting. Relief mapping (Policarpo et al., 2005) can be easily generalized to compute the intersection of a ray with the surface implicitly encoded by distance maps built from arbitrary projections. The classic approach for relief mapping is to compute the ray-heightfield intersection by sampling points along the ray, first using linear search to find a sample inside the object, and then refining the intersection point through binary search, Figure 7(a). For each sampled point, the height of the sample is compared with the depth stored in the relief map to determine whether the sample is inside or outside the heightfield. This idea can be trivially extended from heightfields to distance maps constructed from the projection types discussed in Section 3.2. We also sample points P_i along the ray, see Figure 7(b). Each sample P_i is projected onto the corresponding domain face to compute the projected point P_i' which is converted to local (u_i,v_i) coordinates. The distance value d stored at (u_i,v_i) is dequantized and then compared with the distance $||P_i - P'||$ to check whether the sampled point is inside or outside the object. The distribution of tasks between the different processors is as follows.

The CPU-based part of the rendering algorithm proceeds through the following steps:

1. Bind the array textures encoding distance/color/normal maps to different texture units, and bind also the texture encoding the LUT of cubic cells and projection types to another texture unit.

2. Draw the frontfaces of the G cells, just to ensure that a fragment will be generated for any viewing ray intersecting the underlying object.

The vertex shader performs no significant computations. The most relevant part of the rendering relies on the fragment shader, which performs these steps:

1. Compute the viewing ray.
2. Sample points on the ray using linear search to find the first sample, if any, inside the object. For each sample point, we identify the cell c containing the sample, retrieve the projection $\mathcal{P}$ associated with the cell, and apply $\mathcal{P}$ to project the sample onto domain face. Stop as soon as a sample inside the object is found. Otherwise, the ray does not intersect the surface and hence the fragment is discarded.
3. Refine the intersection point using binary search, as in classic relief mapping.
4. Use the texture coordinates (u,v) at the intersection point to lookup surface signals such as color and normal data.

Most acceleration methods for relief mapping can be also adopted to our approach. In particular, interval mapping can be integrated into our approach with little effort.

4 RESULTS

We have implemented a prototype version of the proposed algorithms and we have tested them with detailed models from the Aim@Shape repository.

Table 1 shows full construction times, including the computation of the cells intersected by the mesh and the sampling process required to build the distance and normal maps. Note that these times are highly competitive and clearly outperform construction times of state-of-the-art parameterization algorithms. The storage space required to store the array textures has been computed using 2 bytes to quantize distance values (Table 1). In all cases a low-resolution grid was enough to obtain a parameterization with little or no overlap between mesh triangles.

Figure 8 shows the results of our raycasting rendering algorithm. Note that differences are hardly noticeable. Rendering times measured on an Nvidia GTX 280 are shown in Table 2. Rendering times are clearly dominated by the number of fragments to be processed. How these rendering times compare to rendering the input model depends basically on the complexity of the model and its screen projection.

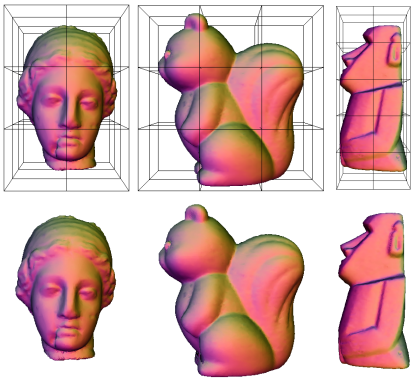

Figure 8: Results using raycasting rendering (bottom row) compared with the original model (top row)

	Egea	Squirrel	Moai	Pensatore
Frame rate	107 fps	112 fps	99 fps	111 fps
Rays/s	28M	29M	26M	29M

Table 2: Rendering times using raycasting on a 512x512 viewport, and number of ray-surface intersections.

Simple models with large screen projections are rendered much faster using the original mesh, whereas complex models with small screen projection render much faster with our output-sensitive approach. Table 2 also shows the number of ray intersections that can be computed per second. It is worth to remark that the ray throughput we achieve also holds for reflected and refracted rays. The rendering time for drawing the model as is or its reflection on a curved mirror is roughly proportional to the number of ray intersections. This unique feature makes our approach particularly suitable for ray-tracing in the GPU. Note that competing representations such as relief-mapped meshes only perform well once the fragment coordinates and interpolated texture coordinates have been computing during the rasterization stage; otherwise, additional spatial data structures are required to compute the ray-mesh intersection.

Unlike polycube maps (Tarini et al., 2004), our representation can be computed fully automatically. Furthermore, since the parameterization is implicit and quickly reversible from the distance maps, the original mesh is not required to render the surface, and the surface can be rendered efficiently using a raycasting approach. The simplicity of our approach comes at a price though. Since we leave out optimization steps performed during construction of polycube maps and the flexibility offered by storing explicit texture coordinates, our parameterization might suffer from higher distortion.

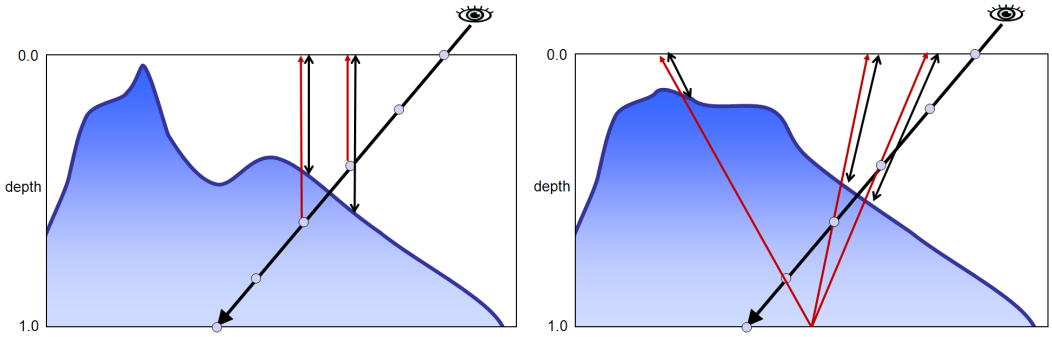

(a) (b)

Figure 7: Computing ray-surface intersections by sampling points along the ray: (a) surface encoded as a heightfield (b) surface encoded using a perspective projection. The red arrows indicate the direction of projection; black arrows show the distance stored in the texture, which is checked against the real distance from the sampled point on ray to the projection plane.

	# Faces	# G cells	# Domain faces	Texture size	Total size	Construction times	
						G cells	Sampling
Egea	16.5K	18	42	64x64	336KB	< 1s	< 1s
Squirrel	20K	18	42	64x64	336KB	< 1s	< 1s
Moai	20K	20	48	64x64	384KB	< 1s	< 1s
Pensatore	1M	1	6	128x128	192KB	2 s	3 s

Table 1: Construction times for the test models.

5 CONCLUSIONS

The main contributions of the paper are (a) a projection-based method for defining implicit parameterization of surface meshes onto an automatically computed set of cubic cells, (b) a unified representation of detailed meshes based on the above parameterization using array textures encoding projection distances and other surface signals such as normals and color, (c) an efficient GPU-based algorithm for sampling these signals, and (d) a rendering algorithm which generalizes relief mapping to arbitrary projections. Since we target GPU-based construction and rendering, we restrict ourselves to easily invertible, implicit projections, at the expense of bijectivity and distortion minimization guarantees. Our approach is oriented towards arbitrarily-detailed models whose main features are roughly well captured by a low resolution grid. Complex surfaces with many thin parts such as bones or pipes might require a high resolution grid to sample faithfully the surface, thus making our approach less attractive for representing these models.

There are several directions that can be pursued to extend the current work. The parameters defining each projection type can be optimized by taking into account the distribution of the geometry inside each G cell, at the expense of higher construction times. For instance, the CoP used by case 0 can be computed as the centroid of the part of the mesh intersecting the cell, instead of taking just the cell's center. We would like to further compare our projection with the projector operator proposed by Tarini et al. (2004). Leaving out further optimization steps, the projector operator is also implicitly defined as in our case. Another obvious extension is to use an octree instead of equal-sized cubic cells. The criteria for grid refinement can be applied for each octree node with little effort. This would result in G cells at different levels and with different texture sizes. Since array textures require each 2D texture layer to have the same size, multiple array textures will be needed, one for each different texture size.

ACKNOWLEDGMENTS

This work has been partially funded by the Spanish Ministry of Science and Technology under grant TIN2007-67982-C02. All test models were provided by the AIM@SHAPE Shape Repository.

REFERENCES

Andujar, C., Boo, J., Brunet, P., Fairen, M., Navazo, I., Vazquez, P., and Vinacua, A. (2007). Omni-directional relief impostors. *Computer Graphics Forum*, 26(3):553–560.

Andujar, C., Brunet, P., and Ayala, D. (2002). Topology-reducing simplification through discrete models. *ACM Transactions on Graphics*, 20(6):88–105.

Baboud, L. and Décoret, X. (2006). Rendering geometry with relief textures. In *Proc. of Graphics Interface*, pages 195–201, Toronto, Canada.

Benson, D. and Davis, J. (2002). Octree textures. *ACM Transactions on Graphics (TOG)*, 21(3):785–790.

Dong, S., Bremer, P.-T., Garland, M., Pascucci, V., and Hart, J. C. (2006). Spectral surface quadrangulation. *ACM Transactions on Graphics*, 25(3):1057–1066.

Donnelly, W. (2005). Per-pixel displacement mapping with distance functions. In *GPU Gems 2: Programming Techniques for High-Performance Graphics and General-Purpose Computation*, pages 123–136.

Eisemann, E. and Décoret, X. (2008). Single-pass gpu solid voxelization for real-time applications. In *GI '08: Proceedings of graphics interface 2008*, pages 73–80.

Floater, M. S. and Hormann, K. (2005). Surface parameterization: a tutorial and survey. In N. A. Dodgson, M. S. F. and Sabin, M. A., editors, *Advances in Multiresolution for Geometric Modelling*, Mathematics and Visualization, pages 157–186. Springer, Berlin.

García, I. and Patow, G. (2008). Igt: inverse geometric textures. *ACM Transactions on Graphics*, 27(5):1–9.

Gu, X., Gortler, S. J., and Hoppe, H. (2002). Geometry images. *ACM Transactions on Graphics*, 21(3):355–361.

Guskov, I., Vidimče, K., Sweldens, W., and Schröder, P. (2000). Normal meshes. In *SIGGRAPH'00*, pages 95–102.

Lee, A. W. F., Sweldens, W., Schröder, P., Cowsar, L., and Dobkin, D. (1998). Maps: multiresolution adaptive parameterization of surfaces. In *SIGGRAPH'98*, pages 95–104.

Lefebvre, S. and Dachsbacher, C. (2007). Tiletrees. In *Proceedings of the 2007 symposium on Interactive 3D graphics and games*, page 31. ACM.

Lefebvre, S., Hornus, S., and Neyret, F. (2005). Octree Textures on the GPU. *GPU gems*, 2:595–613.

Lefohn, A., Sengupta, S., Kniss, J., Strzodka, R., and Owens, J. (2006). Glift: Generic, efficient, random-access GPU data structures. *ACM Transactions on Graphics (TOG)*, 25(1):60–99.

Losasso, F., Hoppe, H., Schaefer, S., and Warren, J. (2003). Smooth geometry images. In *SGP '03: 2003 Eurographics/ACM SIGGRAPH symposium on Geometry processing*, pages 138–145. Eurographics Association.

Peachey, D. (1985). Solid texturing of complex surfaces. *ACM SIGGRAPH Computer Graphics*, 19(3):286.

Perlin, K. (1985). An image synthesizer. *ACM SIGGRAPH Computer Graphics*, 19(3):296.

Policarpo, F. and Oliveira, M. M. (2006). Relief mapping of non-height-field surface details. In *Proc. of ACM Symp. on Interactive 3D Graphics and Games*, pages 55–62.

Policarpo, F., Oliveira, M. M., and Comba, J. (2005). Real-time relief mapping on arbitrary polygonal surfaces. In *Proc. of ACM Symposium on Interactive 3D Graphics and Games*, pages 155–162.

Praun, E., Sweldens, W., and Schröder, P. (2001). Consistent mesh parameterizations. In *SIGGRAPH '01*, pages 179–184.

Purnomo, B., Cohen, J. D., and Kumar, S. (2004). Seamless texture atlases. In *SGP '04: Proceedings of the 2004 Eurographics/ACM SIGGRAPH symposium on Geometry processing*, pages 65–74.

Sheffer, A., Praun, E., and Rose, K. (2006). Mesh parameterization methods and their applications. *Foundations and Trends in Computer Graphics and Vision*, 2(2):105–171.

Tarini, M., Hormann, K., Cignoni, P., and Montani, C. (2004). Polycube-maps. In *SIGGRAPH '04*, pages 853–860.

Tatarchuk, N. (2006). Dynamic parallax occlusion mapping with approximate soft shadows. In *I3D '06: Proceedings of the 2006 symposium on Interactive 3D graphics and games*, pages 63–69.